Mapping RNA−Protein Interactions in Ribonuclease P from *Escherichia coli* Using Electron Paramagnetic Resonance Spectroscopy†

Venkat Gopalan,*,‡,§ Henriette Kühne,|| Roopa Biswas,§ Huimei Li,§ Gary W. Brudvig,⊥ and Sidney Altman‡

Departments of Biology, Molecular Biophysics & Biochemistry, and Chemistry, Yale University, New Haven, Connecticut 06520, and Department of Biochemistry, The Ohio State University, Columbus, Ohio 43210

Received March 27, 1998; Revised Manuscript Received November 4, 1998

ABSTRACT: Ribonuclease P (RNase P) is a catalytic ribonucleoprotein (RNP) essential for tRNA biosynthesis. In *Escherichia coli*, this RNP complex is composed of a catalytic RNA subunit, M1 RNA, and a protein cofactor, C5 protein. Using the sulfhydryl-specific reagent (1-oxyl-2,2,5,5-tetramethyl-Δ^3-pyrroline-3-methyl)methanethiosulfonate (MTSL), we have introduced a nitroxide spin label individually at six genetically engineered cysteine residues (i.e., positions 16, 21, 44, 54, 66, and 106) and the native cysteine residue (i.e., position 113) in C5 protein. The spin label covalently attached to any protein is sensitive to structural changes in its microenvironment. Therefore, we expected that if the spin label introduced at a particular position in C5 protein was present at the RNA−protein interface, the electron paramagnetic resonance (EPR) spectrum of the spin label would be altered upon binding of the spin-labeled C5 protein to M1 RNA. The EPR spectra observed with the various MTSL-modified mutant derivatives of C5 protein indicate that the spin label attached to the protein at positions 16, 44, 54, 66, and 113 is immobilized to varying degrees upon addition of M1 RNA but not in the presence of a catalytically inactive, deletion derivative of M1 RNA. In contrast, the spin label attached to position 21 displays an increased mobility upon binding to M1 RNA. The results from this EPR spectroscopy-based approach together with those from earlier studies identify residues in C5 protein which are proximal to M1 RNA in the RNase P holoenzyme complex.

Structure−function relationships of nucleic acid−protein complexes have been probed using footprinting, photochemical cross-linking, and spectroscopic approaches (*1*−*9*). In this report, we describe an electron paramagnetic resonance (EPR)[1] spectroscopy-based approach to determine if specific residues in the protein subunit are proximal to the RNA subunit of RNase P, a ribonucleoprotein (RNP) complex.

RNase P is an essential and ubiquitous enzyme which catalyzes the maturation of the 5′ termini of tRNAs and functions as an RNP complex in vivo (*10, 11*). In *Escherichia coli*, RNase P consists of a catalytic RNA subunit (M1 RNA, 377 nucleotides) and a small protein cofactor (C5 protein, 119 amino acid residues). The role of C5 protein in RNase P catalysis is distinct from other protein-facilitated RNA-catalyzed reactions in that it enhances the catalytic efficiency and versatility of a catalytic RNA which acts in trans on numerous substrates (*10*−*14*).

Various biochemical and genetic studies have provided insights into structure−function relationships of the two subunits of RNase P from *E. coli* (*15*−*23*). Deletion analysis and cross-linking studies have been used to identify domains in M1 RNA which play a crucial role in catalysis. Biochemical characterization of various mutant derivatives of C5 protein led us to conclude that certain conserved hydrophobic and basic residues in C5 protein are important for its function both in vitro and in vivo (*22, 23*). Although high-resolution structural data on the RNase P holoenzyme are still lacking, biochemical data and comparative sequence analysis have been used to generate computer-aided three-dimensional models of M1 RNA (*24*−*27*). Recently, the tertiary structure of the protein subunit of RNase P from *Bacillus subtilis* was established by X-ray crystallography (*28*).

Understanding the assembly of the RNase P holoenzyme necessitates a knowledge of the spatial orientation of specific parts of the protein cofactor in relation to various domains of the catalytic RNA subunit. Toward this objective, we recently used a sulfhydryl-specific, iron complex of EDTA−2-aminoethyl-2-pyridyl disulfide (EPD-Fe) to convert C5 protein, or its single cysteine-substituted mutant derivatives, into a chemical nuclease that will cleave its cognate RNA ligand, M1 RNA, in the presence of ascorbate and hydrogen peroxide (Gopalan et al., unpublished results). This footprinting method in conjunction with the EPR spectroscopy-

† Research in the laboratory of S.A. is supported by National Institutes of Health Grant GM19422 and Human Frontier Science Program Grant RG 0291. Research in the laboratory of G.W.B. is supported by National Institutes of Health Grants GM32715 and GM36442. Research in the laboratory of V.G. is supported by grants from the Ohio−W. Virginia Affiliate of the American Heart Association and by a Seed Grant from the OSURF.

* Corresponding author: Department of Biochemistry, The Ohio State University, Columbus, OH 43210. Telephone: (614) 292-1332. Email: gopalan.5@osu.edu.

‡ Department of Biology, Yale University.

§ Department of Biochemistry, The Ohio State University.

|| Department of Molecular Biophysics & Biochemistry, Yale University.

⊥ Department of Chemistry, Yale University.

[1] Abbreviations: EPR, electron paramagnetic resonance; MTSL, (1-oxyl-2,2,5,5-tetramethyl-Δ^3-pyrroline-3-methyl)methanethiosulfonate spin label; RNP, ribonucleoprotein; SDSL, site-directed spin labeling.

10.1021/bi9807106 CCC: $18.00 © 1999 American Chemical Society
Published on Web 01/21/1999

Table 1[a]

mutation(s) introduced	sequence of oligonucleotide used for site-directed mutagenesis	name of plasmid
1. C113S	5′ C GCG AGC CAG GCG **GGA** GTG GCG ACG CCA TAA TTT TTC C 3′ (C113S)	pBSC5Sn18
2. S16C, C113S	5′ G CTG GAA AAC GAA AGT GAA CTG **GCA** CGG GGT CAG C 3′ (S16C)	pBSC5Sn1819
3. E106C, C113S	5′ CCC GCG AGC CAG GCG **AGA** GTG GCG ACG CCA TAA TTT **ACA** CAA CGC TTC CGA GAG AGC ACG G 3′ (E106C)	pBSC5Sn1820
4. K54C, C113S	5′ G GGC GCG TCG AAC ATT **GCA** CTT GGC GAC TGT AAG ACC 3′ (K54C)	pBSC5Sn1829
5. K66C, C113S	5′ CG GAA GCT TTC ACG CGT CAG CCG **GCA** AAT CCG ATT GCG 3′ (K66C)	pBSC5Sn1830
6. H44C, C113S[b]	5′ CTG AAT TCG CTG GGG **TGT** CCC CGT ATC GGT CTT ACA GTC GCC (H44C) 3′	pBSC5Sn1834
7. V21C, C113S[c]	5′ GC ACG CTG CGG CTG CTG GAA **GCA** GAA GGT GAA CTG AGA CGG GGT CAG CAG ACG C 3′ (V21C)	pBSC5Sn1851

[a] Since the single-stranded DNA used as the template for site-directed mutagenesis of the C5 gene contains the gene in the sense orientation, the sequences of the oligonucleotides used correspond to the antisense orientation. Two mutations were introduced simultaneously either by using two DNA oligonucleotides or by using single-stranded DNA derived from pBSC5Sn18 as the template DNA for mutagenesis. The boldface letters indicate the codon that was altered. The underlined nucleotides represent changes in the wobble position of the respective codon (i.e., silent mutagenesis) which facilitated rapid restriction analysis-based screening of mutants. [b] See Experimental Procedures for details of the PCR-based method used in constructing this mutant. [c] This mutant was prepared by using the QuikChange kit from Stratagene with pBSC5Sn18 serving as the template DNA. The complement to the DNA oligonucleotide shown in this table was also used for mutagenesis according to the manufacturer's instructions.

based strategy employed in this report facilitates mapping contact sites in nucleoprotein complexes such as RNase P.

EXPERIMENTAL PROCEDURES

Materials. (1-Oxyl-2,2,5,5-tetramethyl-Δ^3-pyrroline-3-methyl)methanethiosulfonate was purchased from Toronto Research Chemicals, Toronto, Canada. 7-Diethylamino-3-[(4′-iodoacetyl)aminophenyl]-4-methylcoumarin was purchased from Molecular Probes. The QuikChange site-directed mutagenesis kit was from Stratagene. Other reagents used in this study were obtained from the indicated commercial sources: restriction enzymes, T4 DNA polymerase, T4 DNA ligase, and T4 polynucleotide kinase were from New England Biolabs; T7 RNA polymerase, RNasin, and M13K07 helper phage were from Promega; nucleoside triphosphates, the Mono S FPLC column, and C50 CM Sephadex were from Pharmacia Biotech; Quick Spin G-50 Sephadex columns were from Boehringer Mannheim; carbenicillin was from Gemini Bioproducts.

Site-Directed Mutagenesis of C5 Protein. The various mutant derivatives of C5 protein (except C5 V21C/C113S and C5 H44C/C113S) were generated using the "oligonucleotide-directed mutagenesis without phenotypic selection" method (*23*, *29*, *30*). The sequences of the DNA oligonucleotides used for mutagenesis are listed in Table 1. DNA oligonucleotides were synthesized either by the Keck Biotechnology Resource Laboratory at Yale Medical School or by GIBCO BRL Life Technologies.

The mutant C5 V21C/C113S was constructed using the QuikChange mutagenesis kit from Stratagene. The plasmid pBSC5Sn18, containing the C113S mutation, was used as the template for mutagenesis. The resulting plasmid, pBSC5Sn1851, contains both the V21C and C113S mutations in the gene coding for C5 protein.

The mutant C5 H44C/C113S was constructed using a PCR-based procedure. The mutation was incorporated in the sense primer for PCR (Table 1). The sense primer and an antisense primer complementary to the 3′ end of the coding region were used to amplify nearly two-thirds of the C5 gene encompassing the *Eco*RI site (at nucleotide position 117, with position 1 referring to the A of the ATG codon) and the stop codon of the C5 gene (ending at position 360). This PCR-generated 260-bp product was then digested with *Eco*RI and *Hin*dIII to yield the desired 100-bp fragment, which was then purified after electrophoresis on a 4% nondenaturing polyacrylamide gel. This 100-bp fragment containing the *Eco*RI and *Hin*dIII overhangs was used to replace the corresponding 100-bp *Eco*RI−*Hin*dIII fragment of the plasmid pBSC5Sn1830 (which encodes the mutant C5 K66C/C113S). The resulting plasmid, pBSC5Sn1834, contains both the H44C mutation introduced by the 100-bp PCR-generated fragment and the C113S mutation that was already present on the pBSC5Sn1830 plasmid.

The presence of the engineered mutation in all the plasmid DNAs was confirmed by DNA sequencing. Subsequently, these plasmid DNAs were used to transform *BL21(DE3) E. coli* cells, and the respective mutant proteins were overexpressed (*20*, *23*).

Overexpression and Purification of Mutant Derivatives of C5 Protein. The wild-type C5 protein was purified from *BL21(DE3)* cells as described previously (*20*, *23*). Overexpression of the mutants was performed in *BL21(DE3)pLysS* cells. To overexpress and purify the various mutants, we transformed *BL21(DE3)pLysS* cells with plasmids encoding the single cysteine-substituted mutant derivatives of C5 protein under the control of a promoter for T7 RNA polymerase transcription. Transformants bearing the various mutants were then grown overnight at 37 °C in LB media supplemented with chloramphenicol (35 μg/mL) and carbenicillin (100 μg/mL). Cultures were re-inoculated the next morning in fresh LB media containing chloramphenicol plus carbenicillin and grown at 37 °C until the OD_{600} was 0.4. The cultures were then induced with 2 mM IPTG. After establishing in small-scale cultures that there was T7 promoter-driven overexpression of the various proteins, large-scale (1 L) cultures were grown to isolate the respective proteins.

The cell pellets from the large-scale cultures were sonicated and then centrifuged at 8000*g* for 10 min to obtain a crude pellet (CP) and a crude extract (CE). The CE was centrifuged at 30000*g* for 30 min to obtain a P30 and an S30 fraction. The cysteine-substituted mutants were present in the CP and also in the P30 (i.e., the pellet obtained after the second centrifugation step). To maximize yield, we isolated the mutant proteins from both insoluble fractions (CP and P30) using the procedure described by Baer et al. (1989).

The mutant derivatives of C5 protein were purified using either Mono S (FPLC column) or gravity flow CM Sephadex

C50 chromatography (*20, 23, 32*). Prior to the loading step, 10 mM DTT was included in the various buffers to keep the protein in its reduced state. The reducing agent was deliberately omitted from the buffer used for elution of the protein from these columns in order to facilitate an accurate determination of the concentration of the accessible sulfhydryl group in the final preparation (*28*). Aliquots from the various fractions eluted from CM Sephadex or Mono S FPLC columns were electrophoresed on SDS−polyacrylamide gels and stained with silver nitrate. Only those fractions which showed high purity (>95%) were pooled, and the stocks were stored at −70 °C. The protein concentration of the various preparations was estimated as described previously (*23*). The accessibility of the thiol group in the various single cysteine-substituted mutant derivatives was assessed using a fluorescence assay by reacting the various protein samples with a thiol-reactive coumarin derivative as described by Wilson and Noller (*33*). The masses of the various mutants were determined by electrospray mass spectrometry and will be described elsewhere (Gopalan et al., unpublished results). There was agreement between the observed and expected values (data not shown).

Modification of C5 Protein or Its Single Cysteine-Substituted Derivatives with MTSL. A stock of 40 mM MTSL was prepared in DMSO and stored as 50-μL aliquots at −20 °C. A fresh tube was thawed and used immediately for each modification of protein samples. Typically, the modification reaction was performed at 4 °C by adding an equimolar amount of MTSL (in DMSO) to 12−24 μM protein (in 50 mM sodium acetate, pH 7.2; 10 mM magnesium acetate; 7 M urea). The modification was performed in two steps: (i) adding half the requisite amount of MTSL, and (ii) subsequently shaking the sample in a nutator at 4 °C for 10 min. These two steps were repeated once again. After the modification reaction was completed, the samples were frozen at −70 °C until further use.

Preparation of RNAs. The plasmid pGEM OTC encoding a fragment of the ornithine transcarbamylase (OTC) mRNA was linearized with *Xho*I while the plasmids pJA2′ and pJA2′ Δ1−54 encoding M1 RNA and Δ1−54 M1 RNA, respectively, were linearized with *Fok*I. These linearized plasmids were transcribed by T7 RNA polymerase and the RNAs subsequently isolated using a Quick Spin column procedure (*16, 20*).

Prior to use in EPR experiments, the RNA samples (prepared by in vitro transcription) were (i) suspended in 10 mM Hepes, pH 7.5, 10 mM magnesium acetate, 400 mM ammonium acetate, 5% (v/v) glycerol, 0.01% (v/v) NP-40; (ii) denatured for 5 min at 65 °C; and (iii) renatured by gradual cooling to room temperature.

Reconstitution of RNase P for EPR Studies. The MTSL-modified protein samples were first dialyzed extensively against 10 mM Hepes, pH 7.5, 10 mM magnesium acetate, 5% glycerol, 0.01% (v/v) NP-40. The concentration of ammonium acetate in the dialysis buffer was either 0.1 or 0.4 M depending on the experiment for which the protein sample was to be used. Denatured/renatured M1 RNA, Δ1−54 M1 RNA, or a fragment of the OTC mRNA was then added to the protein samples to generate a 1:1 complex of RNA−protein. In general, the RNA stocks were kept at very high concentrations (≥100 μM) so that only a very small volume would be added to the spin-labeled protein sample.

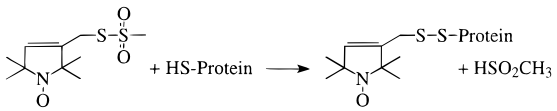

FIGURE 1: Site-directed spin labeling. Reaction of (1-oxyl-2,2,5,5-tetramethyl-Δ^3-pyrroline-3-methyl)methanethiosulfonate (MTSL) with a protein having an accessible cysteine residue enables covalent attachment of the nitroxide spin label to the cysteine residue.

This approach ensured that the protein concentration remained almost unchanged after addition of the desired RNA.

EPR Spectroscopy. Room-temperature X-band EPR spectroscopic measurements were performed on a Bruker EPR spectrometer equipped with a TM_{110} cavity and interfaced to a Macintosh IIci computer. For each measurement, approximately 30 μL of sample was transferred to a glass capillary and placed in a standard quartz EPR sample tube.

EPR spectra were collected under the following conditions: microwave frequency, 9.78 GHz; microwave power, 20 mW; modulation amplitude, 2.5 G; scan time, 20 s; instrumental time constant, 200 ms. Power saturation measurements were performed on both the free spin label and the MTSL-labeled C5 protein to demonstrate that the microwave powers used were nonsaturating (data not shown). Slower scan times and shorter time constants were sampled to justify that the spectra collected under these conditions were not distorted. Details pertaining to data analysis are provided in the respective figure legends.

RESULTS

Site-Directed Spin Labeling (SDSL) of Wild-Type C5 Protein and Its Mutant Derivatives. SDSL involves genetically engineering a cysteine residue in a protein, rendered void of native cysteine residues by mutagenesis, and subsequently modifying the engineered sulfhydryl with a thiol-specific reagent containing a spin label (*34*; Figure 1). The room-temperature EPR spectrum of a spin label is sensitive to its motional freedom and therefore varies as a function of its local environment. Indeed, the nitroxide spin label used in this study has been employed successfully to examine the structure and topography of membrane proteins as well as protein folding (*34*−*37*). We designed the following experiments based on the premise that if the nitroxide spin label in C5 protein was present at the RNA−protein interface, its EPR spectrum would be altered on binding of the spin-labeled C5 protein to M1 RNA.

To introduce the nitroxide spin label at specified sites, we modified with MTSL the single cysteine residue at position 113 in the wild-type C5 protein (Figure 2A) and in the six single cysteine-substituted mutants (S16C/C113S, V21C/C113S, H44C/C113S, K54C/C113S, K66C/C113S, and E106C/C113S) in each of which a Cys was introduced at a defined position and the wild-type Cys113 had been mutated to Ser. The mutant C5 V21C/C113S was the only single cysteine-substituted mutant that was designed based on the recently established tertiary structure of the protein subunit of *B. subtilis* RNase P. All other cysteine replacements were carried out, prior to publication of the tertiary structure, at sites proximal to highly conserved residues whose mutation resulted in moderate or severe loss of function of the protein cofactor (*22*). For instance, Ser16 was mutated to Cys owing to its proximity to Phe18, a highly conserved residue in the

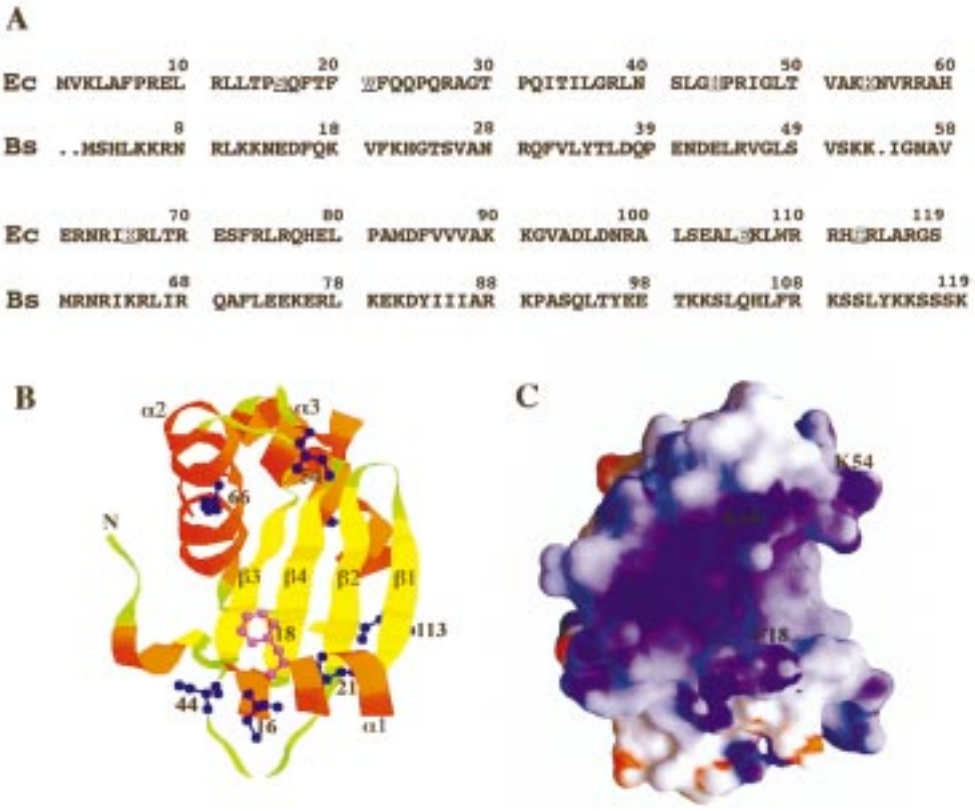

FIGURE 2: (A) Alignment of the amino acid sequences of the protein subunits of RNase P from *E. coli* and *B. subtilis*. The underlined residues indicate sites of cysteine replacements and spin labeling in the protein subunit of *E. coli* RNase P. (B) The tertiary structure of the protein subunit of RNase P from *B. subtilis* (*28*). The α-carbon backbone of the protein structure is depicted as a ribbon. The various secondary structural elements are identified. The positions where Cys residues were introduced and modified with MTSL are indicated in blue; the numbering is based on the sequence of the protein subunit of *E. coli* RNase P. This figure was generated by the program RASMOL using coordinates that were kindly provided to us by Dr. David Christianson, University of Pennsylvania. The program QUANTA′97 *Protein Design* (Molecular Simulations Inc., San Diego) was used to generate the structure of the RNase P protein subunit in which the native amino acid residues at the indicated positions in the *B. subtilis* protein were replaced with a cysteine residue; the coordinates published by Stams et al. (*28*) served as the starting template. (C) Electrostatic potential mapped to the molecular surface of the protein depicted in panel B; this figure was prepared using GRASP (*42, 43*). To reveal the putative RNA-binding cleft in panel C, the view in panel B was rotated to the right by approximately 45°. Blue and red shading represents regions of the surface where positive and negative electrostatic potential would map, respectively. To orient the reader while comparing panels B and C, selected residues are indicated in both panels.

amino acid sequences of the protein subunits of RNase P from bacteria (*23*). The observation that M1 RNA reconstituted with the mutant C5 F18A results in a mutant holoenzyme displaying altered substrate specificity (compared to the wild-type holoenzyme) suggests that Phe18 might be involved in binding to M1 RNA (*23*).

As a test of whether the modification procedure resulted in attachment of the spin label at the specified cysteine residues, we used mass spectrometry to determine the molecular masses of wild-type C5 protein (with a cysteine residue at position 113) and its various single cysteine-substituted mutant derivatives before and after treatment with MTSL. There was agreement between the observed and expected values for the masses of the various proteins before and after modification with MTSL (data not shown).

Prior to performing any EPR experiments, we determined if the cysteine replacements introduced in C5 protein and their subsequent modification with MTSL had any effect on the function of the respective protein. The spin-labeled samples of the wild-type C5 protein and its single cysteine-substituted mutants were reconstituted with wild-type M1 RNA, and the ability of these holoenzymes to cleave the precursor to $tRNA^{Tyr}$ ($ptRNA^{Tyr}$) was examined using in vitro assays as described elsewhere (*23*). The results of the RNase P assays demonstrated that the modification with MTSL resulted in modest effects and did not abolish protein function (at 30 °C) of the wild-type C5 protein or its single cysteine-substituted mutant derivatives (data not shown).

Changes in EPR Spectra Due to Protein Folding. We examined the EPR spectra of wild-type C5 protein and its various mutant derivatives in the presence of 7 M urea (Figure 3A). The EPR spectrum of the free spin label in aqueous buffer is provided for comparison. A comparison of the EPR spectra of free MTSL versus the various spin-labeled protein samples in the same buffer confirmed the attachment of the nitroxide spin label to a large molecule such as C5 protein which restricts the mobility of the spin label (albeit slightly). An analysis of the line shapes of the EPR spectra reveals a decrease in the peak height of the high-field line in the EPR spectra of various protein samples. In contrast, the low-, center-, and high-field peak heights observed in the spectrum of free MTSL are identical, as expected for a rapidly tumbling molecule with isotropic motion (Figure 3A).

The EPR spectra of the various folded, spin-labeled protein samples should be distinctive if the spin label was introduced

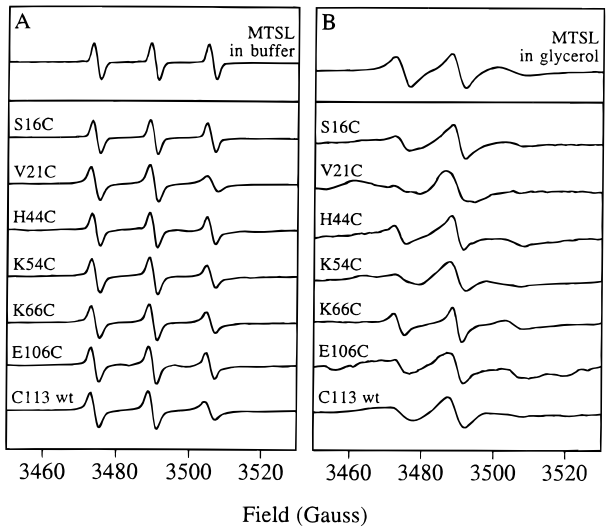

FIGURE 3: Changes in EPR spectra due to protein folding. First-derivative EPR spectra of spin-labeled wild-type C5 protein (Cys113) or its single cysteine-substituted mutant derivatives in the presence of 7 M urea (A) or in 10 mM Hepes, pH 7.5, 10 mM magnesium acetate, 2.4 M ammonium acetate, 5% (v/v) glycerol, 0.01% (v/v) NP-40 (B). Spectra of MTSL in buffer and glycerol are provided as references for comparable label mobility at the top of panels A and B, respectively. All spectra are scaled to the amplitude of the center-field peak to illustrate the changes in line shape.

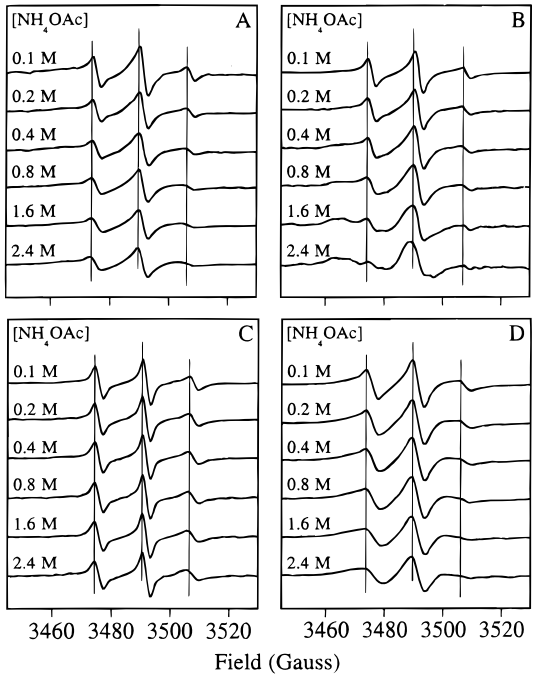

FIGURE 4: Effect of increasing salt concentration on the EPR spectra of Cys16-, Cys21-, Cys66-, and Cys113-MTSL. First-derivative EPR spectra of Cys16-MTSL (A), Cys21-MTSL (B), Cys66-MTSL (C), and Cys113-MTSL (D) in the presence of 10 mM Hepes, pH 7.5, 10 mM magnesium acetate, 5% (v/v) glycerol, 0.01% (v/v) NP-40, and the indicated concentration of ammonium acetate. All spectra are scaled on the basis of sample concentration.

at positions in the protein which differ in their microenvironment. Indeed, there are significant differences in the EPR spectra of the various spin-labeled protein samples that we examined under nondenaturing conditions in the presence of high salt (Figure 3B). The EPR spectrum of the free label in glycerol, which is expected to exhibit slower tumbling than in aqueous solution, is provided for comparison (Figure 3B). Comparison of the EPR spectra of a given spin-labeled sample in the presence and absence of urea (Figure 3A versus 3B) reveals changes in the spectral profiles concomitant with protein folding. In general, the sharp spectrum indicative of a mobile spin label in the denatured state of the protein is replaced by a broadened spectrum resulting from a partially immobilized spin label in the folded protein (Figure 3B). The extent of broadening is different for the various spin-labeled proteins. This is to be expected since protein folding will lead to differences in the extent to which a side chain is buried or exposed. For instance, the spectrum of V21C-MTSL is indicative of a side chain that is highly restricted, perhaps due to a close packing of the tertiary structure proximal to this residue (see results below). In contrast, the spectrum of K66C-MTSL reveals a spin label with higher mobility, consistent with the spin label located in a surface-exposed position.

It is well established that an increase in the ionic strength leads to strengthened hydrophobic interactions in proteins (*38*). Therefore, we investigated the EPR spectra of some of the spin-labeled mutant derivatives of C5 protein as a function of salt concentration (Figure 4). Recently, the tertiary structure of the protein subunit of RNase P from *B. subtilis* was determined by X-ray crystallography (*28*). Since there is nearly 30% sequence identity between the protein subunits of RNase P from *E. coli* and *B. subtilis*, it is reasonable to expect that these two proteins will exhibit structural homology. Based on this premise, Val21 in helix α1 of C5 protein is expected to be part of the hydrophobic interface generated by packing of helix α1 against the central β-sheet (Figure 2B). In contrast, Ser16 in helix α1 of C5 protein will be exposed to the solvent (Figure 2B). Therefore, the salt-induced changes in the EPR spectra of Cys16-MTSL and Cys21-MTSL are expected to be different. Indeed, the results confirm this postulate. As the salt concentration in the buffer was increased from 0.1 to 2.4 M, we observed progressive immobilization of the spin label at position 21 presumably due to increased hydrophobic interactions between helix α1 and the β-sheet (Figure 4B). When a similar experiment was performed to examine if a salt-induced broadening was observed in the EPR spectrum of Cys16-MTSL, we observed modest changes in the EPR spectrum as a function of increasing salt concentration (Figure 4A).

Although Ser16 in helix α1 is exposed to the solvent, it is important to bear in mind that helix α1 is part of a hydrophobic interface with the central β-sheet. This could account for the modest salt-induced broadening observed with Cys16-MTSL. It is likely that tertiary-structure context influences the salt-induced effects on the EPR spectra of surface-exposed residues. In fact, such an expectation is borne out by the EPR spectra of the spin label attached to another surface-exposed residue (Lys66) in helix α2. Increasing ionic strength elicited negligible changes in the EPR spectrum of Cys66-MTSL (Figure 4C).

We recently postulated that Trp109 is in an aromatic cluster which is important for the structure and function of C5 protein (*23, 24*). Based on the prediction that Trp109 and Cys113 are in an α-helix in C5 protein and that both these residues are buried, we investigated the EPR spectrum of the spin label attached to Cys113 as a function of salt

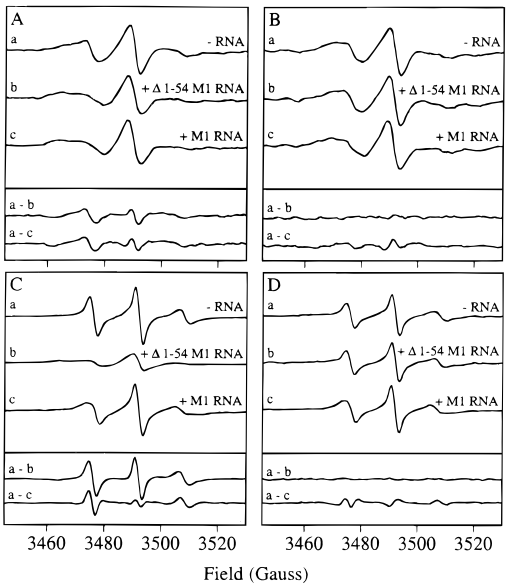

FIGURE 5: Specificity in RNase P complex formation. The EPR spectra of Cys113-MTSL (A, B) and Cys66-MTSL (C, D) in the absence and presence of M1 RNA or Δ1−54 M1 RNA in 10 mM Hepes, pH 7.5, 10 mM magnesium acetate, 5% (v/v) glycerol, 0.01% (v/v) NP-40 containing 0.4 M ammonium acetate (A, C) or 2.4 M ammonium acetate (B, D). All spectra are scaled on the basis of sample concentration. The difference spectra depicted in the bottom of each panel are empirical measures of the line shape changes.

concentration. As the salt concentration in the buffer was increased from 0.1 to 2.4 M, we observed progressive immobilization of the spin label at position 113 (Figure 4D). In the folded protein, the spin label attached to Cys113 is significantly immobilized even at low ionic strength (i.e., 0.1 M ammonium acetate) compared to the protein in 7 M urea (Figure 3A versus Figure 4D). Nevertheless, there is significant additional broadening of the spectrum as the salt concentration is increased from 0.1 to 2.4 M. However, the extent of salt-induced broadening observed with Cys113-MTSL is less than that observed with Cys21-MTSL.

Changes in EPR Spectra Due to RNA Binding. To determine if the spin label attached to various positions in C5 protein is present at the RNA−protein interface, the EPR spectra of the spin-labeled wild-type C5 protein and its single cysteine-substituted mutant derivatives were examined in the absence or presence of M1 RNA. To establish specificity of interaction in the EPR experiments, we chose to compare the results obtained with M1 RNA to those observed with Δ1−54 M1 RNA, a mutant derivative of M1 RNA in which the first 54 nucleotides of M1 RNA have been deleted and which fails to display any activity in the absence or presence of C5 protein (*16, 21*).

Using MTSL-labeled samples in the buffer used for RNase P assays in vitro, we observed that the inactive deletion mutant Δ1−54 M1 RNA was capable of causing significant changes in the line shape of the EPR spectra of almost all the spin-labeled samples used in this study. The changes observed in the EPR spectra of Cys113- and Cys66-MTSL upon addition of M1 RNA or Δ1−54 M1 RNA are illustrated in Figure 5A,C. Although this deletion mutant is inactive and fails to form a functional complex with C5 protein (at subnanomolar concentrations used in the RNase P assay), its addition leads to a significant broadening of the EPR spectra of Cys113- and Cys66-MTSL (at micromolar concentrations) similar to that observed with M1 RNA. In fact, the same result was observed when another RNA, a 450-nt fragment derived from the 5′ end of the coding region of ornithine transcarbamylase (OTC) mRNA, was added to the Cys113- and Cys66-MTSL protein samples (data not shown). These data indicate that an ill-defined, nonspecific interaction occurs between any RNA and the spin-labeled protein at micromolar concentrations in a buffer that contains 0.4 M ammonium acetate.

While using a gel-retardation assay to measure dissociation constants for assembly of the RNase P holoenzyme, Talbot and Altman (*21*) noted that at concentrations of C5 protein higher than 40 nM, a nonspecific aggregate of protein and RNA was observed in the wells of the gel. Since the concentration of protein used for the EPR experiments was at least 12−24 μM, it is possible that the high concentrations of RNA and protein might permit formation of nonspecific complexes between C5 protein and nonspecific RNAs. By increasing the concentration of salt to 2.4 M ammonium acetate, we sought to disrupt such nonspecific complexes. Under these conditions, the EPR spectra obtained with Cys113-MTSL and Cys66-MTSL in the absence or presence of Δ1−54 M1 RNA reveal no changes (Figure 5B,D). However, with the specific ligand M1 RNA, changes in the EPR spectra of Cys113-MTSL and Cys66-MTSL do occur at the high concentration of ammonium acetate (Figure 5B,D). We therefore decided to perform the RNA binding experiments for our EPR study at 2.4 M ammonium acetate.

After analysis of the line shape of the EPR spectra of the spin label attached to Cys16, Cys21, Cys44, Cys54, Cys66, Cys106, and Cys113 in the absence and presence of a specific or nonspecific RNA (Figures 5 and 6), the following inferences can be drawn. First, M1 RNA, but not Δ1−54 M1 RNA, causes a noticeable broadening of the spectra of the nitroxide spin label attached to Cys16, Cys44, Cys54, Cys66, and Cys113. These data suggest that there is an increased immobilization of the spin label attached to positions 16, 44, 54, 66, and 113 in C5 protein upon binding to M1 RNA, but not Δ1−54 M1 RNA. Second, the nature and extent of change in the EPR spectra induced by the RNA ligand are variable as reflected in the various difference spectra (Figures 5 and 6). Third, there is a marked sharpening of the EPR spectrum of Cys21-MTSL upon binding to M1 RNA, presumably due to an increase in the mobility of the spin label upon formation of the RNase P holoenzyme (Figure 6B). Last, the spectrum of Cys106-MTSL is unchanged upon addition of M1 RNA or Δ1−54 M1 RNA (Figure 6E). It is important to appreciate that the low quality of the EPR spectrum of Cys106-MTSL might have obscured modest changes that accompany RNP complex formation.

Since the amplitudes of the peaks are altered as the peaks broaden, we calculated the ratio of the peak-to-peak amplitudes observed for both the low-field ($m_I = -1$) and center-field ($m_I = 0$) peaks in the absence and presence of M1 RNA or Δ1−54 M1 RNA (Table 2). The low- and center-field amplitude ratios confirm the broadening or sharpening of EPR spectra induced by M1 RNA (Table 2). The high-field peaks ($m_I = 1$) were broad and of low amplitude. Since the determination of the amplitudes of such peaks is associated with a high error, the values for the high-field peaks are not reported.

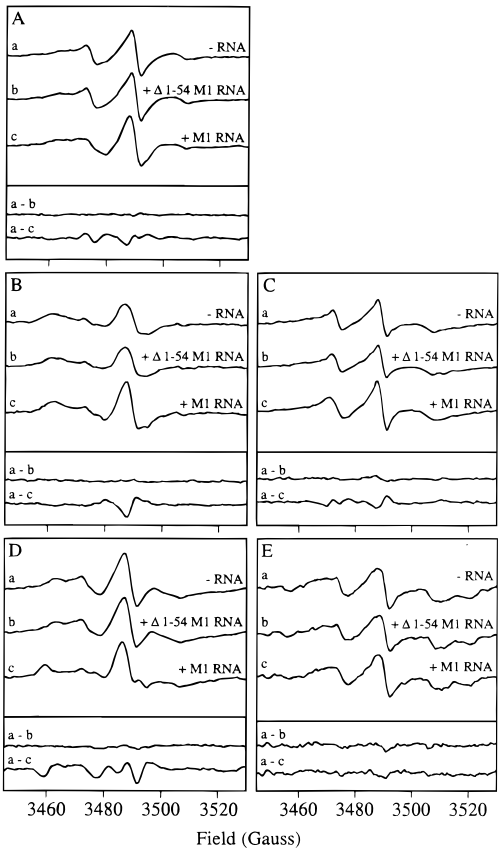

FIGURE 6: Changes in EPR spectra upon RNA binding. The EPR spectra for Cys16-MTSL (A), Cys21-MTSL (B), Cys44-MTSL (C), Cys54-MTSL (D), and Cys106-MTSL (E) in the absence and presence of M1 RNA or Δ1−54 M1 RNA [in 10 mM Hepes, pH 7.5, 10 mM magnesium acetate, 5% (v/v) glycerol, 0.01% (v/v) NP-40, 2.4 M ammonium acetate] are provided. All spectra are scaled on the basis of sample concentration. The difference spectra are shown in the bottom of each panel.

The difference spectra (Figures 5 and 6) as well as the ratio of the amplitudes of the peaks (Table 2) are empirical measures of the line shape changes. They are provided merely to contrast the broadening of the line shape observed upon addition of M1 RNA, but not Δ1−54 M1 RNA, to the various spin-labeled protein samples.

DISCUSSION

Using a site-directed spin labeling procedure and EPR spectroscopy, we have determined that certain residues in the protein subunit of RNase P are at or proximal to the RNA−protein interface in RNase P from *E. coli*. The conclusions with regard to contact sites in the RNP complex are based on identifying positions in the protein subunit where a covalently attached spin label displays a decreased mobility/flexibility in the presence of the cognate RNA ligand.

We first confirmed that a nitroxide spin label was introduced individually at defined positions in the protein subunit of RNase P (Figure 3). Subsequently, we verified that this modification did not eliminate the activity of the RNase P holoenzyme reconstituted in vitro with M1 RNA (the catalytic subunit of RNase P) and the MTSL-modified protein subunit (data not shown).

The EPR spectra of the spin label attached to positions 16, 21, 44, 54, 66, 106, and 113 in C5 protein exhibit marked differences (Figure 3B). There are relatively sharp peaks in the EPR spectra of Cys44- and Cys66-MTSL in contrast to the more broadened spectra observed with Cys16-, Cys21-, Cys54-, Cys106-, and Cys113-MTSL. The distinctive EPR spectra indicate differences in the local environment of the spin label at various positions in the folded protein. Based on these data, we conclude that the spin label attached to the various positions is increasingly mobile in the following order: Cys21 < Cys54 < C113 = Cys106 < Cys16 < Cys44 < Cys66; this gradation in mobility is attributable to differences in the local flexibility of the spin label. Recently, the tertiary structure of the protein subunit of RNase P from *B. subtilis* was determined (*28*). Assuming that the high degree of sequence identity between the protein subunits of RNase P from *E. coli* and *B. subtilis* would translate into a structural homology, we can interpret the EPR spectra of the spin label attached to positions 16, 21, 44, 54, 66, 106, and 113 in C5 protein. With the exception of Cys54, the gradation in mobility of the spin label (indicated above) is consistent with the respective positions of the spin label in the tertiary structure of the protein subunit of RNase P (Figure 2B). Cys54 is placed in the turn between strand β3 and helix α2; the spin label attached to Cys54 is immobilized to a degree greater than that expected for a residue positioned in a turn (see discussion below). The residues Cys21, Cys106, and Cys113 either point inward toward the core or are involved in hydrophobic interactions; hence, the structural rigidity of the spin label attached to these positions is not unexpected. Cys44 and Cys66 are likely to be solvent-exposed, and, therefore, it is not surprising that the spin label attached to these positions displays the least immobilization.

Table 2: Peak Height Ratios from EPR Spectra of Spin-Labeled Wild-Type C5 Protein or Its Single Cysteine-Substituted Mutant Derivatives in the Presence of either Δ1−54 M1 RNA or M1 RNA[a]

spin-labeled protein and RNA used to obtain EPR spectra	low-field peak I/I_o	center-field peak I/I_o
1. C5 S16C/C113S		
+ Δ1−54 M1 RNA	0.89 ± 0.04	0.91 ± 0.05
+ M1 RNA	0.60 ± 0.09	0.91 ± 0.06
2. C5 V21C/C113S		
+ Δ1−54 M1 RNA	0.85 ± 0.05	1.02 ± 0.11
+ M1 RNA	1.60 ± 0.27	1.86 ± 0.32
3. C5 H44C/C113S		
+ Δ1−54 M1 RNA	1.02 ± 0.07	0.99 ± 0.02
+ M1 RNA	0.78 ± 0.07	0.99 ± 0.04
4. C5 K54C/C113S		
+ Δ1−54 M1 RNA	1.00 ± 0.09	0.98 ± 0.04
+ M1 RNA	0.62 ± 0.22	0.90 ± 0.25
5. C5 K66C/C113S		
+ Δ1−54 M1 RNA	0.98 ± 0.05	1.00 ± 0.01
+ M1 RNA	0.75 ± 0.06	0.94 ± 0.09
6. C5 E106C/C113S		
+ Δ1−54 M1 RNA	0.90 ± 0.03	1.13 ± 0.33
+ M1 RNA	0.98 ± 0.03	1.14 ± 0.15
7. C5 C113 (wild type)		
+ Δ1−54 M1 RNA	1.03 ± 0.09	1.01 ± 0.06
+ M1 RNA	0.81 ± 0.04	0.97 ± 0.07

[a] The I/I_o values represent the ratio of the amplitudes observed in the presence and absence of the respective RNA for a given spin-labeled sample. The ratios are provided both for the low-field ($m_I = -1$) and for the center-field ($m_I = 0$) lines. The amplitudes were scaled for differences in concentration or signal intensity; the I/I_o values from both approaches were comparable. The mean and standard deviation values were calculated on the basis of data from three independent experiments. Individual spectra were reproducible.

The observation that Cys16 is part of helix α1, which is involved in hydrophobic interactions with the β-sheet, might account for the increased immobilization of the spin label attached to the solvent-exposed Cys16 compared to the spin label attached to Cys44 and Cys66.

We identified conditions which enabled us to discriminate between the specific and nonspecific RNA binding displayed by C5 protein as examined by EPR spectroscopy (Figure 5). Δ1−54 M1 RNA, an inactive deletion derivative of M1 RNA, was chosen as a negative control since this RNA was not expected to bind C5 protein in a manner similar to M1 RNA. Contrary to our expectation that this RNA would cause negligible changes in the EPR spectra of the spin-labeled protein samples, we observed significant broadening of the EPR spectra of the spin-labeled samples in the presence of Δ1−54 M1 RNA (at low salt concentrations). This indicated that there was an interaction between the spin-labeled protein samples and Δ1−54 M1 RNA. It is important to consider that the concentration of protein (12−24 μM) used in our EPR experiments was nearly 3 orders of magnitude higher than that used previously in a gel-retardation assay in which a similar nonspecific interaction was observed between M1 RNA and C5 protein (*21*). By increasing the concentration of ammonium acetate from 0.4 to 2.4 M in the buffer used in our EPR experiments, we were able to completely eliminate the interaction between micromolar concentrations of Δ1−54 M1 RNA or OTC mRNA and C5 protein (Figure 5 and data not shown). We note, however, that the RNase P holoenzyme loses activity at high ammonium acetate concentrations (such as 1.4 M) in in vitro assays performed with nanomolar concentrations of C5 protein and M1 RNA (data not shown). Nevertheless, we performed the RNA binding experiments for our EPR study at 2.4 M ammonium acetate since our EPR data revealed that it was possible to dissociate nonspecific complexes that can assemble from micromolar concentrations of protein and RNA.

Upon addition of M1 RNA, we observe broadening of the EPR spectra of C5 Cys16-, Cys44-, Cys54-, Cys66-, and Cys113-MTSL, but little or no broadening in the spectrum of Cys106-MTSL. The differential broadening of the EPR spectra indicates that the nitroxide label attached to C5 protein at positions 16, 44, 54, 66, and 113 is immobilized to varying degrees upon addition of M1 RNA but not with Δ1−54 M1 RNA. In contrast, the EPR spectrum of Cys21-MTSL is sharpened upon addition of M1 RNA and not Δ1−54 M1 RNA; this reflects an increase in the mobility of the spin label attached to position 21 in the RNase P complex compared to the spin label in the uncomplexed protein (see discussion below).

Results similar to those obtained in this study have been observed in earlier investigations wherein spin-labeled nucleic acid molecules were used to study the structure of nucleoprotein complexes (*8, 9, 39*). While studying by EPR spectroscopy the encapsidation of spin-labeled poly(A) by tobacco mosaic virus (TMV) protein to form viral-like particles, a pronounced broadening of the EPR spectra was observed during in vitro assembly of the viral-like particle (*8*). Another study examining the binding of bacteriophage fd gene 5 protein to spin-labeled polynucleotides revealed a significant change in the EPR line shape upon formation of the DNA−protein complex (*9*). Finally, a complex of *Eco*RI bound to spin-labeled DNA oligonucleotides (containing the recognition site for *Eco*RI) was investigated by EPR spectroscopy to determine the conformational changes in the DNA that occur upon binding to *Eco*RI (*39*). The changes in spectral line shapes were used to infer that a spin label positioned proximal to the GAATTC recognition site is indeed influenced by the binding event (*39*). In each of the above-mentioned studies, the degree to which the EPR spectra changed upon formation of the respective nucleoprotein complex was different; however, the change always involved a broadening of the EPR spectra. These data were interpreted to reflect an increase in the ordering of the environment around the spin label in the nucleoprotein complex compared to the free, spin-labeled nucleic acid (*8, 9, 39*).

The immobilization of the spin label (in C5 protein) which occurs upon binding of C5 protein to M1 RNA could result from either conformational changes in the protein, which impede the motion of the spin label, or local ordering in the protein induced by RNA−protein interactions in the RNP complex. The results from the EPR spectroscopy-based method fail to distinguish between these two possibilities. However, we discuss below data from other studies, including the recent crystal structure of the RNase P protein subunit, which in conjunction with results from this EPR spectroscopy-based study offer some insights on the spin-labeled residues that are part of the RNA−protein interface in RNase P.

The structure of the protein subunit of *B. subtilis* RNase P reveals that most of the conserved residues are present in two regions: (i) helix α2 as well as the loop which precedes it in the βαβ left-handed crossover motif; and (ii) the large central cleft which is formed by packing of helix α1 against the β-sheet (Figure 2B; *28*). The binding of RNA to the surface of a β-sheet is a common theme in the RNA−protein complex structures reported so far in the literature (*40*). In the tertiary structure of the protein subunit of *B. subtilis* RNase P, a large cleft is formed by packing of helix α1 against the central β-sheet. The surface electrostatic potential map of this protein reveals that the binding cleft is rich in conserved, positively charged residues (Figure 2C). Conserved aromatic residues reside in the helix at the base of the cleft. Therefore, this large cleft with basic and aromatic residues offers an ideal binding site for an RNA molecule. Indeed, mutagenesis of conserved residues such as Phe18, Phe22, Arg62, and Lys66 (which line the cleft in C5 protein) did result in an alteration of *E. coli* RNase P activity (*23*).

Upon identifying the rare left-handed crossover in the βαβ motif of the protein subunit of RNase P, Stams et al. (*28*) postulated that the unfavorable topology must have been conserved through evolution to fulfill important functional requirements. It is therefore reasonable to expect that conserved residues in the βαβ motif of C5 protein (such as Lys54 in the turn connecting β3 to α2) might play an important role in the function of the RNase P protein subunit. Consistent with this expectation, the EPR spectra of Cys54-MTSL in the absence and presence of M1 RNA indicate increased immobilization of Cys54-MTSL in the RNase P holoenzyme. Also, the spin label attached to position 66 (in helix α2) displays a decreased mobility upon binding to M1 RNA. Taken together, we conclude that the basic residues (lining the cleft) play an important role in RNA recognition (see Figure 2C). However, a detailed biochemical evaluation

of the contribution of individual residues in the $\beta\alpha\beta$ motif as well as the central cleft to RNase P catalysis is necessary.

The *rnpA49* mutation (i.e., C5 R46H) results in a temperature-sensitive phenotype in *E. coli*. It has been demonstrated that assembly of the mutant RNase P holoenzyme is defective when C5 R46H is reconstituted with M1 RNA (*32*). Based on the rationale that Arg46 is important for assembly of the RNase P holoenzyme, we introduced a cysteine residue and a spin label at position 44 to examine if this region of the C5 protein is involved in RNA−protein interactions. There is a modest difference in the mobility of the spin label upon binding of the spin-labeled protein (Cys44-MTSL) to M1 RNA.

In a recent footprinting study, we covalently tethered EDTA-Fe to Cys16 in C5 protein and observed hydroxyl radical-mediated cleavages in the P3 helix of M1 RNA (Gopalan et al., unpublished results); this result led us to conclude that in the RNase P holoenzyme complex, residue 16 in C5 protein must be proximal to the P3 helix of M1 RNA. The EPR spectroscopic data reveal a broadening of the EPR spectra of Cys16-MTSL upon binding to M1 RNA (Figure 6A). The results from the footprinting and EPR spectroscopic studies both indicate that Cys16 is at or proximal to the RNA−protein interface although Cys16 points away from the cleft lined with basic and aromatic residues (Figure 2B).

According to the tertiary structure of the protein subunit of RNase P from *B. subtilis*, the Cys residues at positions 16 and 44 would not be part of the central cleft (Figure 2B,C). The observations that the EPR spectra of Cys16- and Cys44-MTSL are slightly broadened in the presence of M1 RNA suggest that RNA contacts may not be limited to the residues lining the central cleft.

When EDTA-Fe was covalently tethered to Cys106 or Cys113 in C5 protein, we did not observe any hydroxyl radical-mediated cleavages in M1 RNA. Therefore, we concluded that both Cys106 and Cys113 are distal to the RNA−protein interface (Gopalan et al., unpublished results). This observation is consistent with the failure to see any changes in the EPR spectrum of Cys106-MTSL in the presence and absence of M1 RNA (Figure 6E). However, there is a modest decrease in the mobility of the spin label attached to Cys113 upon binding to M1 RNA (Figure 5B). An explanation consistent with results from these two approaches would be that conformational changes occur inside the core of the protein (at or proximal to Cys113) as a consequence of binding to M1 RNA and that Cys113 does not represent a contact site in the RNP complex. Although the results from the footprinting and EPR spectroscopy-based approaches suggest that residues 106 and 113 might not be part of the RNA−protein interface, it is possible that other proximal residues in the same helix $\alpha3$ (for example, Arg111) might still contact the RNA subunit.

In contrast to the M1 RNA-induced broadening observed with the spectra of Cys16-, Cys44-, Cys54-, and Cys66-MTSL, there is a marked sharpening of the EPR spectrum of Cys21-MTSL upon binding to M1 RNA (Figure 6B). We interpret this as indicative of an increase in the mobility of the spin label (attached to position 21) upon formation of the RNA−protein complex and as evidence of a conformational change around Val21 in C5 protein which likely weakens the interaction of helix $\alpha1$ and the β-sheet. This result needs to be viewed in context of what is known about residues surrounding position 21, as well as RNA binding-induced conformational changes observed in other RNA-binding proteins (*40*, *41*).

Phe18 and Phe22 are conserved and semiconserved residues, respectively, in the amino acid sequences of the protein subunits of RNase P from bacteria (*23*). The observation that M1 RNA reconstituted with the mutant C5 F18A or C5 F22A results in a mutant holoenzyme displaying altered substrate specificity (compared to the wild-type holoenzyme) suggests that these residues might be involved in binding to M1 RNA and RNase P catalysis (*23*). Consistent with this expectation, we have observed that the mutant C5 F18A also displayed weaker binding to M1 RNA compared to the wild-type C5 protein (Gopalan et al., unpublished results). In the tertiary structure of the protein subunit of RNase P from *B. subtilis*, there is a hydrophobic interface between helix $\alpha1$ and the β-sheet (*28*). The corresponding hydrophobic interface in C5 protein, the protein subunit of *E. coli* RNase P, comprises Phe18, Val21, Phe22, Leu36, and Val86. If the aromatic residues are involved in RNA binding and in base stacking in the RNA−protein complex, are these residues exposed to the solvent in the free, unbound protein? It is instructive to examine an analogous situation in the structure of the spliceosomal protein U1A complexed with its RNA ligand (*40*, *41*).

A comparison of the high-resolution structures of the human spliceosomal protein U1A in the absence and presence of its RNA ligand (U1 RNA hairpin II) revealed structural rearrangements concomitant with RNP complex formation. Pertinent to this discussion is the position of the C-terminal helix C in U1A in the free and bound structures (*40*, *41*). Helix C lies across the surface of the β-sheet involved in RNA binding and has been referred to as a lid on the RNA-binding surface. Such an interaction stabilizes the protein by ensuring that the hydrophobic residues are not exposed to the solvent. However, upon binding to the RNA, the helix changes its orientation by 135°, thereby facilitating interactions between the hydrophobic residues in the β-sheet and the RNA ligand. Drawing a parallel to the structural rearrangements in U1A which occur upon RNA binding, we envision that binding to M1 RNA induces conformational changes in the interface between helix $\alpha1$ and the β-sheet of C5 protein. Such a change would be consistent with the M1 RNA binding-induced increase in the mobility of the spin label attached to position C21 in C5 protein.

The EPR spectroscopy-based approach described in this report could be used as a primary screen to identify cysteine residues, engineered or otherwise, that are proximal to the RNA−protein interface in an RNP complex. Subsequently, the residues of interest could be modified with photoactivatable cross-linking reagents (such as azidophenazyl bromide) or footprinting reagents (such as EDTA-Fe) to obtain more information regarding the regions in the RNA that are contacted by these residues. An extension of this study would be to examine the EPR spectra of an RNP complex reconstituted with RNA and protein subunits each having a single nitroxide spin label attached to it at a defined position. If the spin labels in the two subunits were within 20 Å of each other, the resultant spin−spin interactions could be used to calculate distances between defined positions in the RNA and protein subunits.

ACKNOWLEDGMENT

We are grateful to Dr. Cecilia Guerrier-Takada and Daniel Pomeranz Krummel for helpful discussions and critical reading of the manuscript, and Dr. David Christianson, University of Pennsylvania, for providing us the coordinates for the tertiary structure of the protein subunit of RNase P from *B. subtilis*. We thank Drs. Dieter Söll and Craig Crews for the use of the FPLC systems in their laboratories. Electrospray mass spectrometric analysis was kindly performed by Dr. David Ledman, Sealy Center for Structural Biology, University of Texas Medical Branch, Galveston, TX. We thank Dr. K. McGrath for providing us with the pGem OTC clone. During his tenure at Yale, V.G. was supported by postdoctoral fellowships from the Patrick and Catherine Donaghue Foundation for Medical Research and the Anna Fuller Fund for Cancer Research.

REFERENCES

1. Tullius, T. D. (1987) *Trends Biochem. Sci. 12*, 297−300.
2. Bastia, D. (1996) *Structure 4*, 661−664.
3. Wilson, K. S., & Noller, H. F. (1998) *Cell 92*, 131−139.
4. Meisenheimer, K. M., & Koch, T. H. (1997) *Crit. Rev. Biochem. Mol. Biol. 32*, 101−140.
5. Urlaub, H., Thiede, B., Müller, E.-C., Brimacombe, R., & Wittmann-Liebold, B. (1997) *J. Biol. Chem. 272*, 14547−14555.
6. Foster, M. P., Wuttke, D. S., Case, D. A., Gottesfeld, J. M., & Wright, P. E. (1997) *Nat. Struct. Biol. 4*, 605−608.
7. Tan, R., & Frankel, A. D. (1994) *Biochemistry 33*, 14579−14585.
8. Hilhorst, H. W. M., Postma, U. D., & Hemminga, M. A. (1982) *FEBS Lett. 142*, 301−304.
9. Bobst, A. M., Ireland, J. C., & Bobst, E. V. (1984) *J. Biol. Chem. 259*, 2130−2134.
10. Altman, S., Kirsebom, L., & Talbot, S. J. (1995) in *tRNA: Structure, Biosynthesis and Function* (Söll, D., & RajBhandary, U., Eds.) pp 67−78, American Society for Microbiology, Washington, DC.
11. Pace, N. R., & Brown, J. W. (1995) *J. Bacteriol. 177*, 1919−1928.
12. Reich, C., Olsen, G. J., Pace, B., & Pace, N. R. (1988) *Science 239*, 179−182.
13. Peck-Miller, K., & Altman, S. (1991) *J. Mol. Biol. 221*, 1−5.
14. Tallsjo, A., & Kirsebom, L. A. (1993) *Nucleic Acids Res. 21*, 51−56.
15. Guerrier-Takada, C., Lumelsky, N., & Altman, S. (1989) *Science 286*, 1578−1584.
16. Guerrier-Takada, C., & Altman, S. (1992) *Proc. Natl. Acad. Sci. U.S.A. 89*, 6383−6387.
17. Haas, E. S., Brown, J. W., Pitulle, C., & Pace, N. R. (1994) *Proc. Natl. Acad. Sci. U.S.A. 91*, 2527−2531.
18. LaGrandeur, T. E., Hüttenhofer, A., Noller, H. F., and Pace, N. R. (1994) *EMBO J. 13*, 3945−3952.
19. Harris, M. E., & Pace, N. R. (1995) *RNA 1*, 210−218.
20. Vioque, A., Arnez, J., & Altman, S. (1988) *J. Mol. Biol. 202*, 835−848.
21. Talbot, S. J., & Altman, S. (1994) *Biochemistry 33*, 1399−1405.
22. Gopalan, V., Golbik, R., Schreiber, G., Fersht, A., & Altman, S. (1997) *J. Mol. Biol. 267*, 765−769.
23. Gopalan, V., Baxevanis, A., Landsman, D., & Altman, S. (1997) *J. Mol. Biol. 267*, 818−829.
24. Westhof, E., & Altman, S. (1994) *Proc. Natl. Acad. Sci. U.S.A. 91*, 5133−5137.
25. Harris, M. E., Nolan, J. M., Malhotra, A., Brown, J. W., Harvey, S. C., & Pace, N. R. (1994) *EMBO J. 13*, 3953−3962.
26. Westhof, E., Wesolowski, D., & Altman, S. (1996) *J. Mol. Biol. 258*, 600−612.
27. Massire, C., Jaeger, L., & Westhof, E. (1998) *J. Mol. Biol. 279*, 773−793.
28. Stams, T., Niranjanakumari, S., Fierke, C., and Christianson, D. W. (1998) *Science 280*, 752−756.
29. Kunkel, T. A. (1985) *Proc. Natl. Acad. Sci. U.S.A. 82*, 488−492.
30. Kunkel, T. A. (1989) in *Current Protocols in Molecular Biology* (Ausubel, F. M., Brent, R., Kingston, R. E., Moore, D. D., Seidman, J. G., Smith, J. A., & Struhl, K., Eds.) pp 8.1.1−8.1.6, John Wiley, New York.
31. Kirsebom, L. A., Baer, M. F., and Altman, S. (1988) *J. Mol. Biol. 204*, 879−888.
32. Baer, M. F., Wesolowski, D., & Altman, S. (1989) *J. Bacteriol. 171*, 6862−6866.
33. Wilson, K. S., and Noller, H. F. (1998) *Cell 92*, 131−139.
34. Hubbell, W. L., Mchaourab, H. S., Altenbach, C., & Lietzow, M. A. (1996) *Structure 4*, 779−783.
35. Altenbach, C., Marti, T., Khorana, H., & Hubbell, W. L. (1990) *Science 248*, 1088−1092.
36. Voss, J., Salwinski, L., Kaback, H. R., & Hubbell, W. L. (1995) *Proc. Natl. Acad. Sci. U.S.A. 92*, 12295−12299.
37. Voss, J., Hubbell, W. L., & Kaback, H. R. (1995) *Biochemistry 37*, 211−216.
38. Kennedy, R. M. (1990) *Methods Enzymol. 182*, 339−343.
39. Keyes, R. S., Cao, Y. Y., Bobst, E. V., Rosenberg, J. M., & Bobst, A. M. (1996) *J. Biomol. Struct. Dyn. 14*, 163−172.
40. Varani, G., & Nagai, K. (1996) *Annu. Rev. Biophys. Biomol. Struct. 27*, 407−445.
41. Avis, J. M., Allain, F. H.-T., Howe, P. W. A., Varani, G., Nagai, K., & Neuhaus, D. (1996) *J. Mol. Biol. 257*, 398−411.
42. Nicholls, A., Sharp, K. A., & Honig, B. (1991) *Proteins: Struct., Funct., Genet. 11*, 281−296.
43. Nicholls, A. (1993) *GRASP: Graphical representation and alignement of surface properties*, Columbia University, New York.

BI9807106